Recent Development and Application of the Linear Matching Method for Design Limits in Plasticity and Creep: An Overview

Haofeng Chen and Weihang Chen

Abstract Engineering design and integrity assessment of components under the action of cyclic thermal and mechanical loading require the assessment of load histories for which certain types of material failure do not occur. This involves the determination of the shakedown limit, ratchet limits, plastic strain range concerning fatigue crack initiation in a low cycle fatigue assessment, and creep fatigue interaction.

In this paper a state-of-the-art direct method, the Linear Matching Method (LMM), is summarized for the evaluation of these design limits in both plasticity and creep. These have been solved by characterizing the steady cyclic state using a general cyclic minimum theorem. For a prescribed class of kinematically admissible inelastic strain rate histories, the minimum of the functional for these design limits are found by either global minimization process or dual minimization process. The applications of the LMM to three practical problems are outlined to confirm the efficiency and effectiveness of the method and demonstrate that Direct Methods may be applied to a much wider range of circumstances than have hitherto been possible.

Keywords Plasticity · Creep · Direct methods · Cyclic loading · Shakedown · Ratchetting · Creep-fatigue interaction

1 Introduction

Imperfections in structures can arise in the initial production process, or during the heat-treatment of the component, particularly during welding processes. These defects or flaws are unavoidable within structure components, and they do not generally lead to an immediate failure. Failure modes occurring from these structures are different from industry to industry, but mostly such failures result from the application of cyclic loading with high temperature. In general, the lifetimes of these components, operating at elevated temperatures, depend on the nature of plastic

H. Chen (✉) · W. Chen
Department of Mechanical and Aerospace Engineering, University of Strathclyde, Glasgow G1 1XJ, UK
e-mail: haofeng.chen@strath.ac.uk

K. Spiliopoulos, D. Weichert (eds.), *Direct Methods for Limit States in Structures and Materials*, DOI 10.1007/978-94-007-6827-7_13,
© Springer Science+Business Media Dordrecht 2014

and creep deformation they experience. The first failure mode is mainly concerned with the excessive plastic deformations associated with the phenomenon of plastic collapse, shakedown and ratchetting, while the second is concerned with the creep fatigue interaction. The ability to accurately model these behaviours of component subjected to cyclic and variable loading conditions would provide a means of assessing the remaining life of the structural components. Thus, the elastic-plastic-creep response of a structure needs to be well understood when using it as a design condition.

The determination of these design limits has attracted the attentions of many researchers. The phenomena of shakedown and ratchetting associated with the steady cyclic response have been researched and modeled extensively by plasticity theorists, materials scientists, mathematicians and engineers. Since closed form solutions of these design limits are very limited due to the complexity of the problem, the numerical approaches play a key role for the assessment of these design limits in plasticity.

One approach is to simulate the detailed elastic-plastic response of the structure for a specified cyclic load history, most commonly by the incremental Finite Element Analysis (FEA) [1]. However, this method requires significant computer time for complex structures, due to the reason of its investigation of any load cycle. A relatively new cyclic analysis method, Direct Cyclic Analysis (DCA) [2], has been developed to avoid excessive numerical expense associated with the incremental FEA. It has been recently incorporated into ABAQUS to evaluate the stabilized cyclic behaviour directly. However, both the incremental FEA and DCA do not predict shakedown or ratchet limits directly. It can only be used to show whether elastic shakedown, plastic shakedown or ratchetting occurs [3].

To define the shakedown and ratchet limits, alternative approach has been developed. It involves the application of numerical methods [4–9] for addressing the structural response in structures subjected to both severe mechanical and thermal loads. The assessments, provided from these new methods, have the potential of providing results that combine the accuracy of non-linear FEA simulation methods [10, 11] with the efficiency of rules-based methods [12, 13]. These are direct methods based upon a programming technique. Direct methods were incorporated into finite element analysis in order to evaluate the shakedown limit. The material model is considered to be elastic perfectly plastic, and the load domain including all the possible load paths eliminates the necessity to know the detailed load history. Such direct methods include; the mathematical programming methods [14–16], the Generalized Local Stress Strain (GLOSS) r-node method [17], the Elastic Compensation Method (ECM) [18], and the Linear Matching Method (LMM) [7, 19, 20]. Among these direct methods, the LMM is counted to be the method most amenable to practical engineering applications involving complicated thermomechanical load history. The LMM has been extensively applied to a range of problems [8, 19], through various adaptations, extended to the calculation required for the UK assessment procedure R5 [21] for the high temperature response of structures. The LMM describes non-linear inelastic material behaviour by linear solutions where the material coefficients vary both spatially and in time, which makes the method

particularly flexible. The LMM has been regarded as an efficient and effective upper bound programming method for which, in many circumstances, strict convergence proofs may be constructed. In the past two years, the LMM has been further developed to account for the lower bound shakedown and ratchets limits, and investigate more complicated cyclic problems. Moreover, the extensions of LMM have resulted in the application of the method to high temperature creep behavior including the effect of elastic follow-up [20], i.e. the evaluation of local creep damage due to the relaxation of stress during creep dwell times.

There are four objectives leading to using the basics of these methods in this study where limit in plasticity and creep are designed. The first objective is to obtain a LMM approach used for more general purposes. This LMM must be able to address to a wider class of problems and prospective procedures for lower and upper bound design limits. The second objective is to assess the cyclic response under creep fatigue conditions by presenting a new numerical procedure. The third is the examination and the improvement of convergence problems existing in the iterative approach and the last objective is to validate the efficiency and effectiveness of LMM while designing the limits in plasticity and creep. This validation is performed on three typical practical problems. The first problem is; a defective pipeline subjected to cyclic thermal loading and constant operating pressure. In the second problem the effects of drilling holes on the ratchet limit and crack tip plastic strain range for a central cracked plate subjected to constant tensile loading and cyclic bending moment are investigated, and in the last one the cyclic structural responses of a cruciform weldment under creep fatigue interaction is being addressed.

In the following sections, a general cyclic minimum theorem for perfect plasticity and the application of the LMM for a particular class of problems for the design limits in plasticity and creep will be described. This is followed by the discussion of convergence and the application of three practical examples with numerical verifications of the proposed methods.

2 Cyclic Behaviour

2.1 General Cyclic Problem

Consider a body with volume V and surface S, where the material is isotropic, elastic-plastic and satisfies the von Mises yield condition. A cyclic history of temperature $\lambda\theta(x,t)$ occurs within volume V. A cyclic load history $\lambda P(x,t)$ is applied over part of S, namely S_T. Here λ denotes a scalar load parameter. On the remainder of S, namely S_u, zero displacements are maintained. Both load and temperature histories have the same cycle time Δt and, in the following, we are concerned with the behaviour of the body in a typical cycle $0 \le t \le \Delta t$ in a cycle state. For the problem defined above the stresses and strain rates will asymptote to a cyclic state where

$$\sigma_{ij}(t) = \sigma_{ij}(t + \Delta t), \qquad \dot{\varepsilon}_{ij}(t) = \dot{\varepsilon}_{ij}(t + \Delta t). \tag{1}$$

This arbitrary asymptotic cyclic history may be expressed in terms of three components, the elastic solution, a transient solution accumulated up to the beginning of the cycle and a residual solution that represents the remaining changes within the cycle. The linear elastic stress solution is denoted by $\lambda\hat{\sigma}_{ij}$. The general form of the stress solution is given by

$$\sigma_{ij}(x,t) = \lambda\hat{\sigma}_{ij}(x,t) + \bar{\rho}_{ij}(x) + \rho^r_{ij}(x,t) \tag{2}$$

where $\bar{\rho}_{ij}$ denotes a constant residual stress field in equilibrium with zero surface traction on S_T and corresponds to the residual state of stress at the beginning and end of the cycle. The history ρ^r_{ij} is the change in the residual stress during the cycle and satisfies;

$$\rho^r_{ij}(x,0) = \rho^r_{ij}(x,\Delta t). \tag{3}$$

It is worth noting that the arguments in this section do not explicitly call on the properties of perfect plasticity and are therefore common to all cyclic states associated with inelastic material behaviour.

2.2 Description of Design Limits in Plasticity and Creep Under Cyclic Loading

2.2.1 Design Limits in Plasticity

One well-known illustration defining the plasticity limit of the structure under cyclic load history is Bree interaction diagram [22, 23]. Bree [22, 23] developed theoretical solutions for a simplified 2-dimensional model of a nuclear reactor fuel can. In his model, constant pressure stress and cyclic temperature gradient was applied across the can wall during start-up and shutdown. These theoretical solutions were illustrated on Bree interaction diagram in order to provide different modes of material behaviour for different cyclic loading conditions. These diagrams with various cyclic loading combinations are helping the designers especially in their early stages of design.

Figure 1 is the Bree diagram [22, 23], illustrating the responses for the case of a fuel can subject to cyclic through-wall thermal stress and a constant internal pressure. The ordinate and abscissa give normalised values of pressure and thermal stress respectively, where the stresses have been normalised against the yield stress of the material. The distinct feature on the interaction diagram is the separation of the different modes of material behaviour. In this particular analysis, the diagram is divided into four design regions, namely:

Pure Elastic Region In this region, it was found that the load level is sufficiently small; the response is purely elastic, no permanent strains are induced, and the structure returns to its original configuration after each load application.

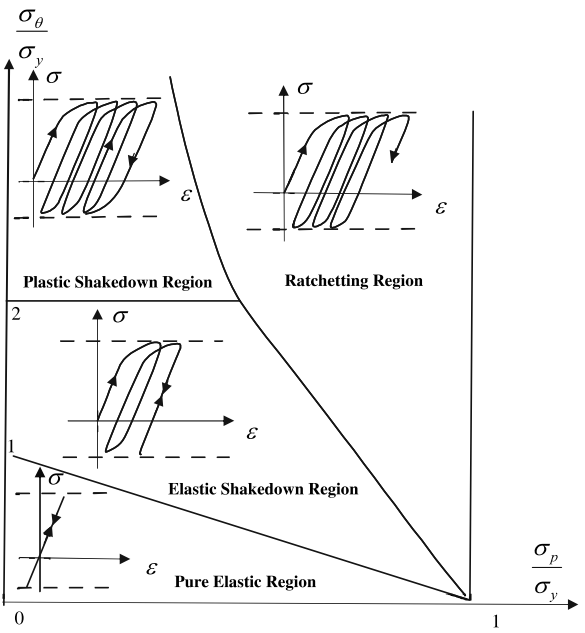

Fig. 1 Bree diagram for pressurized tube and thermal loading [22, 23]

Elastic Shakedown Region In this region, the stresses are exceeding the yield stress at the first few load cycles, which give rise to constant residual stress in the structure such that in subsequent load cycles only elastic deformation occurs. The constant residual stress field has caused the redistribution of the stresses within the structure. This effectively has the effect of pulling the stress fields, the sum of the elastic and residual stresses in to the yield surface.

Reverse Plasticity/Plastic Shakedown Region The transition to this region occurs when the effective elastic stresses exceed twice the yield stress. This was made possible with the accommodation of the time-varying residual stress field, causing the stress distribution at the outer fibre of the plate, to exceed twice the yield stress. When the structure exhibits reverse plasticity over each cycle, the positive plastic strain in the first half of the load cycle followed by equal magnitude negative strain in the second half, such that there is no accumulation of plastic strain during load cycle. And the failure mechanism for plastic shakedown is low-cycle fatigue.

Ratchetting Region This region is best characterized by the breakdown of the elastic, shakedown and reverse-plasticity conditions. In each cycle, plastic strains accumulate over a significant volume of the plate, leading to structural failure from the unlimited accumulation of plastic deformation and eventually incremental plastic collapse.

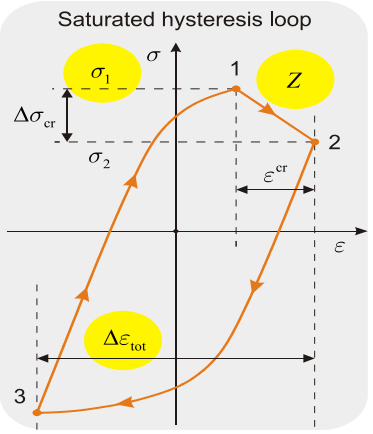

Fig. 2 The Hysteresis cycle which provides the information for fatigue and creep damage

2.2.2 Design Limits in Creep Under Cyclic Loading

In the presence of creep, the response of the structure to cyclic loading changes significantly. Interaction of plasticity and creep is the key feature of creep-fatigue mechanism under cyclic loading condition with creep. Assessments must be carried out to ensure avoidance of creep-fatigue failure by, creep rupture and cyclically enhanced creep. The term cyclically enhance creep refers to the threat of gross section creep failure due to the accumulation of creep strains arising from the cyclic loading. The life design limit under creep fatigue interaction can be defined by construction of stress strain hysteresis loops since this hysteresis loop provides the information of life damage due to fatigue and creep, and this information also is the key to an R5 V2/3 assessment. Figure 2 is the construction of the hysteresis cycle; it provides the total strain range, $\Delta\varepsilon_{tot}$ from which the fatigue damage is calculated, and the start of dwell stress, σ_1 and creep strain, ε^{cr} from which the creep damage is calculated.

3 Minimization Processes of the Linear Matching Method

The strategy of locating each of above critical limits consists of defining an appropriate class of kinematically admissible strain rate histories $\dot{\varepsilon}^c_{ij}$ then solving a corresponding minimizing process for $I(\dot{\varepsilon}^c_{ij}, \lambda)$ by considering the incremental form;

$$I\left(\dot{\varepsilon}^c_{ij}, \lambda\right) = \sum_{n=1}^{N} I^n, \tag{4a}$$

$$I^n\left(\Delta\varepsilon^n_{ij}, \lambda\right) = \int_V \left\{\sigma^n_{ij}\Delta\varepsilon^n_{ij} - \left(\lambda\hat{\sigma}_{ij}(t_n) + \rho_{ij}(t_n) + \bar{\rho}_{ij}\right)\Delta\varepsilon^n_{ij}\right\} dV, \tag{4b}$$

$$\rho_{ij}(t_n) = \bar{\rho}^0_{ij} + \sum_{l=1}^{n} \Delta\rho_{ij}(t_l), \tag{4c}$$

where $\dot{\varepsilon}_{ij}^{c}$ is replaced by a sequence of increments of strain $\Delta\varepsilon_{ij}^{n}$ occurring at a sequence of N times t_n, $n = 1$ to N, during the cycle. The incremental minimization of $I^n(\Delta\varepsilon_{ij}^{n}, \lambda)$ assumes that the prior history of the residual stress is known and compatibility of the total elastic and plastic strain in the increment is used. $\bar{\rho}_{ij}^{0}$ is the constant element of the changing residual stress $\rho_{ij}(t_n)$ and represents as,

$$\bar{\rho}_{ijM}^{0} = \sum_{n=1}^{N} \Delta\rho_{ij}{}_{1}^{n} + \sum_{n=1}^{N} \Delta\rho_{ij}{}_{2}^{n} + \cdots + \sum_{n=1}^{N} \Delta\rho_{ij}{}_{M-1}^{n} \tag{5}$$

where M represents the total number of cycles. In this section, the linear matching processes for minimization of $I(\dot{\varepsilon}_{ij}^{c}, \lambda)$ are summarized for both the shakedown and ratchet limits.

3.1 Global Minimization for Shakedown Limit

The global minimization of $I(\dot{\varepsilon}_{ij}^{c}, \lambda)$makes use of the compatibility from the sum of the increments of plastic strain over the cycle. When a set of increments $\Delta\varepsilon_{ij}^{nk}$ at kth iteration are assumed known, a linear material can be defined so that linear shear modulus $\bar{\mu}^{nk}$ ensures that the resulting deviatoric stress is at yield, i.e.

$$\frac{2}{3}\bar{\mu}^{nk}\bar{\varepsilon}\left(\Delta\varepsilon_{ij}^{nk}\right) = \sigma_0 \tag{6}$$

where $\bar{\varepsilon}$ denotes the von Mises effective strain.

For shakedown problems, the changing component of residual stress vanishes, i.e. $\rho_{ij}^{r} = 0$. Hence, the cyclic stress history for shakedown problem is given by

$$\sigma_{ij}(x,t) = \lambda\hat{\sigma}_{ij}(x,t) + \bar{\rho}_{ij}(x). \tag{7}$$

A set of linear incremental relationships are then defined by

$$\Delta\varepsilon_{ij}^{n(k+1)\prime} = \frac{1}{2\bar{\mu}^{nk}}\left[\lambda\hat{\sigma}_{ij}'(t_n) + \bar{\rho}_{ij}^{k+1\prime}\right], \qquad \Delta\varepsilon_{kk}^{n(k+1)} = 0 \tag{8}$$

where the upper 'dash' refers to deviatoric components. Summing over the cycle produces a relationship between the compatible strain $\Delta\varepsilon_{ij}^{(k+1)} = \sum_n \Delta\varepsilon_{ij}^{n(k+1)}$ and the constant residual stress $\bar{\rho}_{ij}^{k+1}$with an initial stress state;

$$\Delta\varepsilon_{ij}^{(k+1)\prime} = \frac{1}{2\bar{\mu}^{k}}\left(\sigma_{ij}^{initial\,\prime} + \bar{\rho}_{ij}^{k+1\prime}\right), \qquad \Delta\varepsilon_{kk}^{(k+1)} = 0 \tag{9a}$$

where

$$\frac{1}{\bar{\mu}^{k}} = \sum_{n}\frac{1}{\bar{\mu}^{nk}} \quad \text{and} \quad \sigma_{ij}^{initial} = \bar{\mu}^{k}\sum_{n}\frac{\lambda\hat{\sigma}_{ij}(t_n)}{\bar{\mu}^{nk}}. \tag{9b}$$

The solution of the continuum problem corresponding to Eqs. (9a), (9b) has the property that $I(\Delta\varepsilon_{ij}^{(k+1)}, \lambda) \le I(\Delta\varepsilon_{ij}^{k}, \lambda)$, which is proved by [6].

3.2 Dual Minimization Process for Ratchet Analysis

We consider a structure subjected to a general cyclic load condition, which can be decomposed into cyclic and constant components, i.e. $\hat{\sigma}_{ij}(x,t) = \hat{\sigma}_{ij}^{\Delta}(x,t) + \lambda\hat{\sigma}_{ij}^{\overline{F}}(x)$. The calculation of the ratchet limit includes dual minimization processes, the first an incremental minimization for the evaluation of a cyclic history of residual stresses and plastic strain range in a stable cycle and the second a global minimization for the ratchet limit due to an extra constant load. By decoupling the evaluation of the changing residual stress and the constant residual stress in Eqs. (4a)–(4c), the entire numerical procedure of ratchet analysis includes two steps [24]. The first step is to calculate the history of the changing residual stress associated with the applied cyclic load $\hat{\sigma}_{ij}^{\Delta}(x,t)$ and the corresponding plastic strain ranges for the low cycle fatigue assessment. The second step is to locate the ratchet limit due to the extra constant load $\lambda\hat{\sigma}_{ij}^{\overline{F}}(x)$ as a conventional shakedown analysis where a constant residual stress is evaluated by global minimization (Sect. 3.1) and the elastic stress history is augmented by the changes in residual stress calculated in the first step.

The global minimization process for step 2 of ratchet analysis is as same as the global minimization for shakedown limit in Sect. 3.1. Next a distinct minimization process—incremental minimization is summarized for step 1 of ratchet analysis to evaluate the changing residual stress ρ_{ij}^{r} and the associated plastic strain range corresponding to the cyclic component of the elastic stress $\hat{\sigma}_{ij}^{\Delta}$.

3.2.1 Incremental Minimization for the Varying Residual Stress Field and Plastic Strain Range

The incremental minimization of $I^n(\Delta\varepsilon_{ij}^n, \lambda)$ assumes the prior history of the residual stress is known and compatibility of the total elastic and plastic strain in the increment is used. With an initial estimate of $\Delta\varepsilon_{ij}^n = \Delta\varepsilon_{ij}^{nk}$, a linear modulus is defined by linear matching $\sigma_0 = 2/3\bar{\mu}^{nk}\bar{\varepsilon}(\Delta\varepsilon_{ij}^{nk})$, where the von Mises yield stress σ_0 could be either constant or temperature-dependent.

An incremental linear equation is then defined;

$$\Delta\varepsilon_{ij}^{Tn(k+1)\prime} = \frac{1}{2\mu}\Delta\rho_{ij}^{n(k+1)\prime} + \Delta\varepsilon_{ij}^{n(k+1)\prime}, \tag{10a}$$

$$\Delta\varepsilon_{kk}^{Tn(k+1)} = \frac{1}{3K}\Delta\rho_{kk}^{n(k+1)}, \tag{10b}$$

$$\Delta\varepsilon_{ij}^{n(k+1)\prime} = \frac{1}{2\bar{\mu}^{nk}}\left\{\hat{\sigma}_{ij}^{\Delta}(t_n) + \rho_{ij}(t_{n-1}) + \Delta\rho_{ij}^{n(k+1)}\right\}', \tag{10c}$$

where the prior history of the residual stress is known, i.e.

$$\rho_{ij}(t_{n-1}) = \rho_{ij}(t_0) + \Delta\rho_{ij}^{1} + \Delta\rho_{ij}^{2} + \cdots + \Delta\rho_{ij}^{n-1}, \qquad \rho_{ij}(t_0) = \bar{\rho}_{ij}^{0}. \tag{11}$$

The entire iterative procedure requires a number of cycles, where each cycle contains N iterations associated with N load instances. The first iteration is to evaluate

the changing residual stress $\Delta\rho_{ij}^{1}$ associated with the elastic solution $\hat{\sigma}_{ij}^{\Delta}(t_1)$ at the first load instance. Define $\Delta\rho_{ij}{}_{m}^{n}$ as the evaluated changing residual stress for nth load instance at mth cycle of iterations, where $n = 1, 2, \ldots, N$ and $m = 1, 2, \ldots, M$. At each iteration, the above changing residual stress $\Delta\rho_{ij}{}_{m}^{n}$ is calculated. When the convergence occurs at the Mth cycle of iterations, the summation of changing residual stresses at N time points must approach to zero ($\sum_{n=1}^{N}\Delta\rho_{ij}{}_{M}^{n} = 0$) due to the stable cyclic response. Hence the constant residual stress $\rho_{ij}(t_0) = \bar{\rho}_{ij}^{0}$ over the cycle can also be determined by

$$\bar{\rho}_{ij}^{0} = \sum_{n=1}^{N}\Delta\rho_{ij}{}_{1}^{n} + \sum_{n=1}^{N}\Delta\rho_{ij}{}_{2}^{n} + \cdots + \sum_{n=1}^{N}\Delta\rho_{ij}{}_{M}^{n}. \tag{12}$$

The corresponding plastic strain magnitude occurring at time t_n is calculated by

$$\Delta\varepsilon_{ij}^{P}(t_n) = \frac{1}{2\bar{\mu}^{n}}\left(\hat{\sigma}_{ij}^{\Delta\prime}(t_n) + \rho_{ij}'(t_n)\right) \tag{13}$$

where $\bar{\mu}^{n}$ is the iterative shear modulus and $\rho_{ij}(t_n)$ is the converged accumulated residual stress at the time instant t_n, i.e.

$$\rho_{ij}(t_n) = \bar{\rho}_{ij}^{0} + \sum_{k=1}^{n}\Delta\rho_{ij}{}_{M}^{k}. \tag{14}$$

4 Evaluation of Upper and Lower Bound Limits

4.1 Upper Bound Shakedown and Ratchet Limit

Combining $0 \le I(\Delta\varepsilon_{ij}^{(k+1)}, \lambda) \le I(\Delta\varepsilon_{ij}^{k}, \lambda)$ and Eqs. (4a)–(4c), with ρ_{ij} and $\bar{\rho}_{ij}$ eliminated Based upon the Koiter's theorem [25] the upper bound shakedown limit is given as,

$$I\left(\Delta\varepsilon_{ij}, \lambda^{S}\right) = \int_{V}\sum_{n=1}^{N}\left\{\sigma_{ij}^{n}\Delta\varepsilon_{ij}^{n} - \lambda^{S}\hat{\sigma}_{ij}(t_n)\Delta\varepsilon_{ij}^{n}\right\}dV \ge 0, \tag{15a}$$

i.e.

$$\lambda^{S} \le \frac{\int_{V}(\sum_{n=1}^{N}\sigma_{ij}^{n}\Delta\varepsilon_{ij}^{n})dV}{\int_{V}(\sum_{n=1}^{N}\hat{\sigma}_{ij}(t_n)\Delta\varepsilon_{ij}^{n})dV} = \frac{\int_{V}(\sigma_y\sum_{n=1}^{N}\bar{\varepsilon}(\Delta\varepsilon_{ij}^{n}))dV}{\int_{V}(\sum_{n=1}^{N}\hat{\sigma}_{ij}(t_n)\Delta\varepsilon_{ij}^{n})dV} = \lambda_{UB}^{S}. \tag{15b}$$

Equation (15b) provides a monotonically reducing sequence of upper bound to the shakedown limit, i.e. $\lambda_{UB}^{S(k+1)} \le \lambda_{UB}^{S(k)}$. It is worth noting that a limit load can be calculated by Eq. (15b) as a special case of the shakedown analysis, where the cyclic load condition reduces to monotonic load condition, i.e. $N = 1$.

For the upper bound ratchet limit, the numerical technique can be accommodated within the existing methods of shakedown analysis where the linear elastic solution is augmented by the changing residual stress field, i.e.

$$\hat{\sigma}_{ij} = \lambda \hat{\sigma}_{ij}^{\bar{F}} + \hat{\sigma}_{ij}^{\Delta}(x,t) + \rho_{ij}(x,t) \tag{16}$$

where the history of the residual stress field $\rho_{ij}(t_n)$ associated with the cyclic component of the load history has been calculated by an incremental minimization process (Sect. 3.2.1).

For the von Mises yield condition and the associated flow rule, an upper bound ratchet limit multiplier can be obtained by

$$\lambda_{UB}^{R} = \frac{\int_V \sum_{n=1}^{N} \sigma_y \bar{\varepsilon}(\Delta\varepsilon_{ij}^n) dV - \int_V \sum_{n=1}^{N} (\hat{\sigma}_{ij}^{\Delta}(t_n) + \rho_{ij}(t_n)) \Delta\varepsilon_{ij}^n dV}{\int_V \hat{\sigma}_{ij}^{\bar{F}} (\sum_{n=1}^{N} \Delta\varepsilon_{ij}^n) dV} \tag{17}$$

which gives the capacity of the body subjected to a predefined cyclic load history $\hat{\sigma}_{ij}^{\Delta}(t_n)$ to withstand an additional constant load $\hat{\sigma}_{ij}^{\bar{F}}$ before ratchetting takes place.

4.2 Lower Bound Shakedown and Ratchet Limit

Both the constant residual stress $\bar{\rho}_{ij}(x)$ and varying residual stress $\rho_{ij}^{r}(x,t)$ in Eq. (2) for a stabilised load cycle have been calculated by incremental and global minimization processes. Hence, based upon the lower bound theorem [26], a lower bound of shakedown or ratchet limit can be constructed in the same upper bound procedure by maximizing the lower bound load parameter λ_{LB} under the condition where for any potentially active load/temperature path, the stabilised cyclic stresses in Eq. (2) nowhere violate the yield condition.

As the upper bound iterative process provides a sequence of residual stress fields, a sequence of lower bound at each iteration can be calculated by scaling the elastic solution so that the cyclic stress everywhere satisfies yield. The lower bound of shakedown limit multiplier can be described as:

$$\lambda_{LB}^{s} = \max \lambda_{LB} \tag{18a}$$

$$\text{s.t. } f\left(\lambda_{LB}\hat{\sigma}_{ij}(x,t) + \bar{\rho}_{ij}(x)\right) \le 0. \tag{18b}$$

The lower bound of ratchet limit multiplier can be written as:

$$\lambda_{LB}^{R} = \max \lambda_{LB} \tag{19a}$$

$$\text{s.t. } f\left(\lambda_{LB}\hat{\sigma}_{ij}^{\bar{F}} + \hat{\sigma}_{ij}^{\Delta}(x,t) + \rho_{ij}(x,t) + \bar{\rho}_{ij}(x)\right) \le 0. \tag{19b}$$

5 Numerical Procedures for the Creep Strain and Flow Stress

In the incremental minimization process (Sect. 3.2.1) where the plastic strain amplitudes are evaluated, σ_0 (Eq. (6)) is adopted as the material yield stress. However, when the accumulated creep strain is calculated during the dwell period at the

creep load time instance, σ_0 in Eq. (6) needs to be replaced by the creep flow stress $\sigma_0 = \bar{\sigma}_c$. The creep flow stress is an implicit function of creep strain $\Delta\bar{\varepsilon}^c$ and residual stress $\Delta\bar{\rho}^c$ during the creep dwell period. The detailed numerical procedures for the evaluation of creep strain and flow stress are described in [27, 28] and these processes are summarized as follows:

We assume a time hardening creep constitutive relation:

$$\dot{\bar{\varepsilon}}^c = B\bar{\sigma}^{n^*} t^{m^*} \tag{20}$$

where $\dot{\bar{\varepsilon}}^c$ is the effective creep strain rate, $\bar{\sigma}$ is the effective von-Mises stress, t is the dwell time, and B, m^* and n^* are the creep constants of the material. When $m^* = 0$, the time hardening constitutive equation becomes the Norton's law.

During the relaxation process we assume, at each point in space that an elastic follow up factor Z exists:

$$\dot{\bar{\varepsilon}}^c = -\frac{Z}{\bar{E}}\dot{\bar{\sigma}} \tag{21}$$

where $\bar{E} = 3E/2(1+v)$, E is the Young's modulus and $\dot{\bar{\sigma}} = \dot{\bar{\sigma}}(\sigma_{ij})$.

Combining Eqs. (20) and (21) and integrating over the dwell time, we obtain

$$\frac{B\bar{E}\Delta t^{m^*+1}}{Z(m^*+1)} = \frac{1}{n^*-1}\left\{\frac{1}{(\bar{\sigma}_c)^{n^*-1}} - \frac{1}{(\bar{\sigma}_s)^{n^*-1}}\right\} \tag{22}$$

where $\bar{\sigma}_s$ is the effective value of the start of dwell stress, $\bar{\sigma}_c$ is the effective value of the creep flow stress, and $\bar{\sigma}_c = \bar{\sigma}(\sigma_{sij} + \Delta\rho_{Cij})$. Integrating Eq. (21) gives the effective creep strain during the dwell period Δt as,

$$\Delta\bar{\varepsilon} = -\frac{Z}{\bar{E}}(\bar{\sigma}_c - \bar{\sigma}_s). \tag{23}$$

Combining Eqs. (22) and (23) and eliminating $Z/\bar{E}$ gives

$$\Delta\bar{\varepsilon}^c = \frac{B(n^*-1)\Delta t^{m^*+1}(\bar{\sigma}_s - \bar{\sigma}_c)}{(\frac{1}{\bar{\sigma}_c^{n^*-1}} - \frac{1}{\bar{\sigma}_s^{n^*-1}})(m^*+1)}. \tag{24}$$

For the pure creep where $\bar{\sigma}_s = \bar{\sigma}_c$, the creep strain becomes:

$$\Delta\bar{\varepsilon}^c = \frac{B\bar{\sigma}_s^{n^*}\Delta t^{m^*+1}}{m^*+1}. \tag{25}$$

The creep strain rate $\dot{\bar{\varepsilon}}^F$ at the end of dwell time Δt is calculated by Eqs. (22) and (24):

$$\dot{\bar{\varepsilon}}^F = B(\bar{\sigma}_c)^{n^*}\Delta t^{m^*} = \frac{\Delta\bar{\varepsilon}^c}{\Delta t}\frac{(m^*+1)}{(n^*-1)}\frac{\bar{\sigma}_c^{n^*}}{(\bar{\sigma}_s - \bar{\sigma}_c)}\left(\frac{1}{\bar{\sigma}_c^{n^*-1}} - \frac{1}{\bar{\sigma}_s^{n^*-1}}\right). \tag{26}$$

For the pure creep where $\bar{\sigma}_s = \bar{\sigma}_c$, the creep strain rate $\dot{\bar{\varepsilon}}^F$ becomes:

$$\dot{\bar{\varepsilon}}^F = B(\bar{\sigma}_s)^{n^*}\Delta t^{m^*}. \tag{27}$$

Hence in the iterative process, we begin with current estimated $\bar{\sigma}_c^i, \bar{\sigma}_s^i$ and use Eqs. (24), (26) or (27) to compute a new value of the creep stress $\bar{\sigma}_c = \bar{\sigma}_c^f$ from Eq. (28) to replace $\sigma_0(t_n)$ in the linear matching condition Eq. (6).

$$\bar{\sigma}_c = \left(\frac{\bar{\dot{\varepsilon}}^F}{B \Delta t^{m^*}} \right)^{\frac{1}{n^*}}. \tag{28}$$

6 Convergence Considerations

The necessary condition for convergence and the exact proof for upper bounds are provided by [5, 6]. According to this study, in order to get convergent minimum upper bound limits three conditions must be fulfilled as follows: (1) The material yield surface must be convex; (2) The class of strain rates and the associated strain increments guarantee that the minimum upper bound is limited with this class; (3) The class of selected compatible strain distributions must be adequately extensive to guarantee a satisfactory upper bound.

The first two conditions can be easily satisfied by an appropriate choice of a class of linear materials. Condition (3) is vital to the implementation of the LMM within a finite element scheme. Within the LMM, the equilibrium of the residual stress field ρ_{ij} relies on the class of displacement field Δu_i from which $\Delta \varepsilon_{ij}$ is derived, i.e. ρ_{ij} is in equilibrium if and only if $\int_V \rho_{ij} \Delta \varepsilon_{ij} dV = 0$. Hence, for a given finite element mesh, the process will converge to the least upper bound associated with the FE mesh and within this class of displacement field Δu_i. However, during the FE implementation, the volume integration is not exact but usually depends upon the Gaussian integration to give an exact integral. Hence a point-wise condition is used to replace above equilibrium condition;

$$\sum_{el} \sum_{k} w_k \rho_{ij}^k \Delta \varepsilon_{ij}^k = 0 \tag{29}$$

where w_k are the Gaussian weighting factors at the Gauss integration points.

According to the lower and upper bound theorems, the LMM ensures that the maximum lower bound will be less than the least upper bound. However, unlike the strict convergence of the upper bound, the magnitude of lower bound may not always increase monotonically with iterations. But upon convergence, the maximum lower bound will equal to the least upper bound, where by equilibrium condition (Eq. (29)) the matching condition is applied at Gauss points.

Due to the point-wise condition of equilibrium (Eq. (29)), whereas the deviation from convergence at a few Gauss points has little effect on the upper bound which is determined by volume integrals, the convergence of the upper bound in terms of a particular number of significant figures may allow some deviation from convergence locally. Hence the convergence of lower bound may be affected significantly as it is determined by single Gauss point. Generally the upper bound converges (monotonically) more quickly than the lower bound and the rate of convergence for lower bound depends upon the characteristic of the problem and also the adopted FE

model, such as the complexity of the geometry and boundary conditions, the mesh arrangement, etc. For some cases where the lower bound converges very slowly, the convergence is usually judged entirely in terms of the upper bound. Further investigation of the convergence of the LMM iterative algorithms has been carried out and a separate paper is being prepared for this context.

7 Examples of Applications

In this section, three practical examples of the LMM for differing applications are provided to confirm the efficiency and effectiveness of the method; the behaviour of a defective pipeline subjected to cyclic thermal loading and constant operating pressure, the effects of drilling holes on the ratchet limit and crack tip plastic strain range for a centre cracked plate subjected to constant tensile loading and cyclic bending moment, and the cyclic structural responses of a cruciform weldment under creep fatigue interaction.

7.1 Defective Pipelines Subjected to Cyclic Thermal Loading and Constant Operating Pressure

Figure 3 gives a finite element model of a defective pipeline with four types of slot, where the symmetry boundary conditions are applied to the half section of the model. Such pipes are subjected to particular severe thermal loading, resulting in the possibility of ratchetting or premature failure due to low cycle fatigue.

Figure 4 presents the calculated shakedown and ratchet limit interaction curve for a pipeline with these four types of slots, which clearly shows the effect of part-through slot on the shakedown and ratchet limits. It is observed that any part-through slot significantly reduces the reverse plasticity limit of the pipeline due to the stress concentration caused by the existence of the slot. It is also identified that at different levels of cyclic thermal loading the ratchet limit boundary decreases sharply for a defective pipeline with axial and large area slot and it remains almost constant for small and circumferential slot, compared with a defect-free pipeline. Figure 4 further shows that for the cases of axial and large area slots, the ratchet limit ends at cyclic thermal loading points $\Delta\theta = 4.1\Delta\theta_0$ and $\Delta\theta = 5.5\Delta\theta_0$, respectively, which indicates that when the cyclic thermal loading $\Delta\theta$ beyond these cyclic thermal loading limits ($4.1\Delta\theta$ for axial slot and $5.5\Delta\theta$ for large area slot), any amount of constant internal pressure will result in ratchetting.

A full discussion of the solutions including plastic strain range concerning the fatigue crack initiation and verifications with ABAQUS detailed step-by-step analysis are given by [29]. This example demonstrates that, for these practical industrial problems, the method is capable of providing solutions that are much more illuminating than conventional analysis.

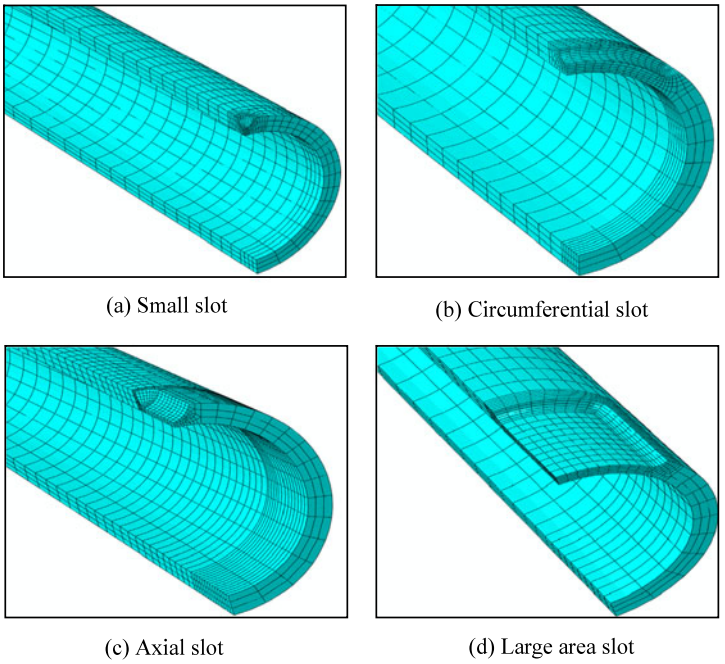

Fig. 3 The finite element mesh for a pipeline with part-through slot: (**a**) small slot; (**b**) circumferential slot; (**c**) axial slot and (**d**) large area slot

Fig. 4 Shakedown and ratchet limit interaction curve for defect-free and defective pipelines

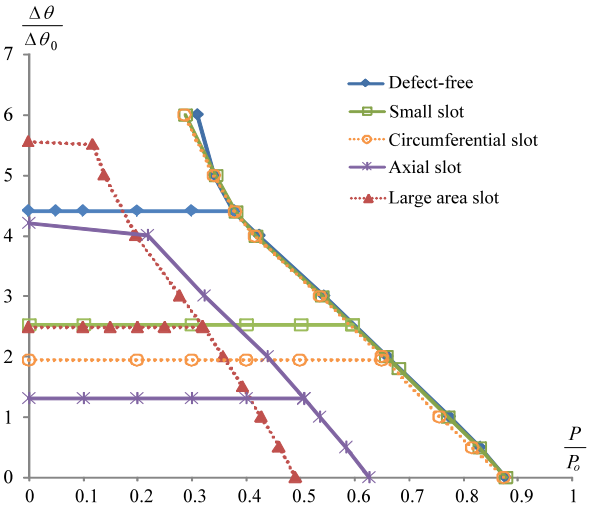

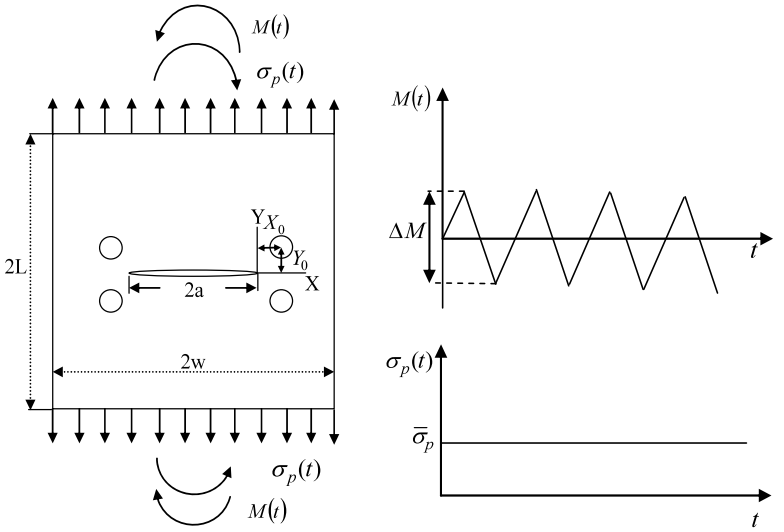

Fig. 5 Centre cracked plate with symmetric holes subjected to reversed bending moment range ΔM and constant tension $\bar{\sigma}_p$

7.2 Centre Cracked Plate with Circular Holes

The second example concerns the effect of circular holes in a centre cracked plate subjected to cyclic bending moment and constant tensile loading on the ratchet limit and crack tip plastic strain range. Drilling holes in front of the crack tip is an effective way to arrest crack growth. However the optimum location and size of the holes need to be researched to produce the smallest crack tip plastic strain range, i.e. the best fatigue crack growth life, and to have the least reduction in ratchet limit.

The geometrical shape and cyclic loading history of the centre cracked plate with symmetric drilled holes are shown in Fig. 5, where the half-crack length a is 500 mm and the ratios W/a and L/a are both 2. The hole locations (X_0, Y_0) are referred to a co-ordinate system X, Y, the origin of which is located at the crack tip. The centre cracked plate is subjected to cyclic reversed bending moment with range ΔM and constant uniaxial tension $\bar{\sigma}_p$. By applying symmetry conditions, a FE half symmetry model was adopted (Fig. 6).

Figure 7 presents the calculated lower and upper ratchet limit and limit load interaction diagram for the hole location at $X/a = -1$, $Y/a = 0.3$ and the diameter of hole $D = 100$ mm, where the applied constant pressure in X-axis is normalized with respect to the reference uniaxial tension $\bar{\sigma}_{po} = 100$ MPa, while the amplitude of the reversed bending moment in Y-axis is normalized using the reference bending moment range $\Delta M_0 = 100$ N mm. It can be seen that the ratchet limit and the limit load curves do not coincide, which means that an increase in the loads beyond the ratchet limit will not automatically cause plastic collapse. Any combination of loads which lies between these two boundaries will result in ratchetting.

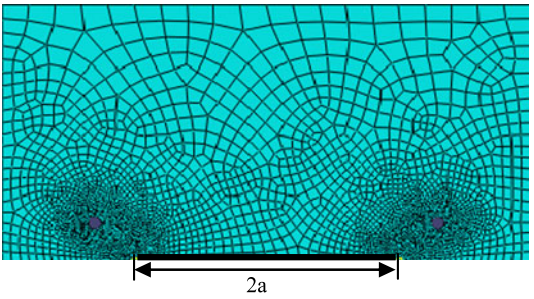

Fig. 6 FE half symmetry model for centre cracked plate with symmetric holes

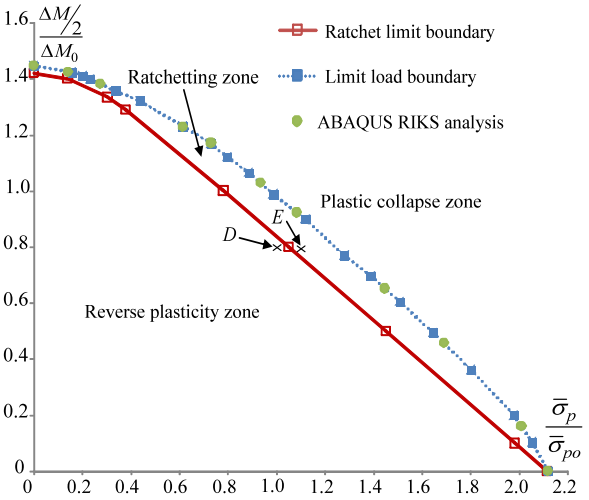

Fig. 7 Ratchet limit and limit load interaction curve with hole location at $\frac{X}{a} = -0.1$, $\frac{Y}{a} = 0.3$ ($D = 100$ mm)

As shown in Fig. 7, the accuracy of the lower and upper bound limit load boundary obtained by the LMM has been verified by ABAQUS RIKS analysis. For the verification of LMM lower and upper bound ratchet limit boundary the cyclic load points D ($\Delta M = 1.6\Delta M_0, \bar{\sigma}_p = \bar{\sigma}_{p0}$), and E ($\Delta M = 1.6\Delta M_0, \bar{\sigma}_p = 1.1\bar{\sigma}_{p0}$), which are just below and above the calculated upper bound ratchet limit boundary (Fig. 7), respectively, are chosen for the step-by-step analysis in ABAQUS.

Figure 8 shows the plastic strain history at the crack tip for the cyclic loading D and E calculated by ABAQUS step-by-step analysis. The calculated plastic strain for the load case D settles to a stable cycle after about 5 load cycles showing a reverse plasticity mechanism, and the load case E shows a strong ratchetting mechanism, with the plastic strain increasing at every cycle. This directly confirms the accuracy of the predicted LMM lower and upper bound ratchet limits.

Optimization studies were performed further involving holes with different diameters drilled at different locations. The study shown that the most significant decrease in crack tip plastic strain range with least reduction in the ratchet limit is identified for the hole size $D = 150$ mm at the optimum location $X_0/a = -0.1$, $Y_0/a = 0.3$, which gives a 72 % reduction in the plastic strain range and does not reduce the ratchet limit.

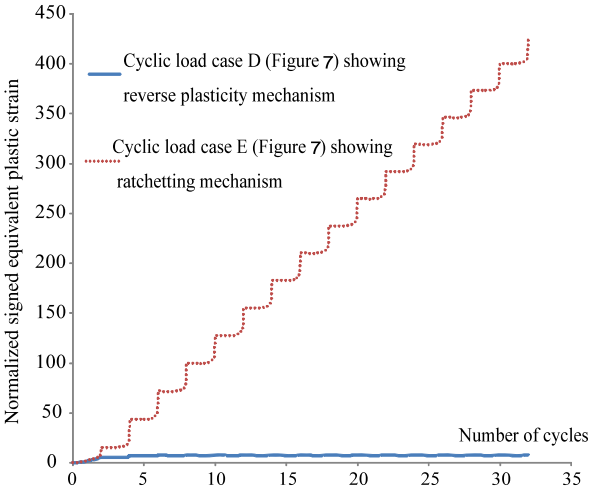

Fig. 8 ABAQUS verification of the ratchet limit for the cyclic bending moment case using detailed step by step analysis

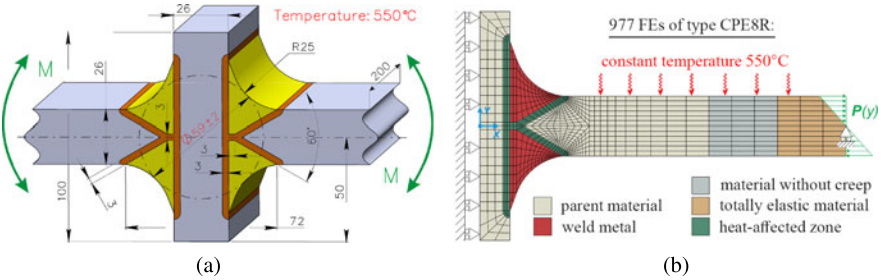

Fig. 9 Geometrical and analysis parameters of the cruciform weld specimens: (**a**) dimensions and applied loading; (**b**) FE-mesh with designation of different materials, boundary conditions and mechanical loading

A full discussion of the solutions is given by [30]. This example demonstrates that the method is capable of providing accurate solutions to the crack structures.

7.3 Creep-Fatigue Analysis of a Cruciform Weldment

The LMM has been extended recently to directly evaluate steady-state cyclic response of components with creep fatigue interaction taking into consideration, which is able to generate both the closed and non-closed hysteresis loops, providing details of creep strain and plastic strain range for creep and fatigue damage assessments. This example shows a practical application of this method on a cruciform weldment subjected to cyclic bending moment under creep condition.

Figure 9 describes the geometry of the weldment specimen and the applied 2D symmetric FE model of the specimen assuming a plane strain condition.

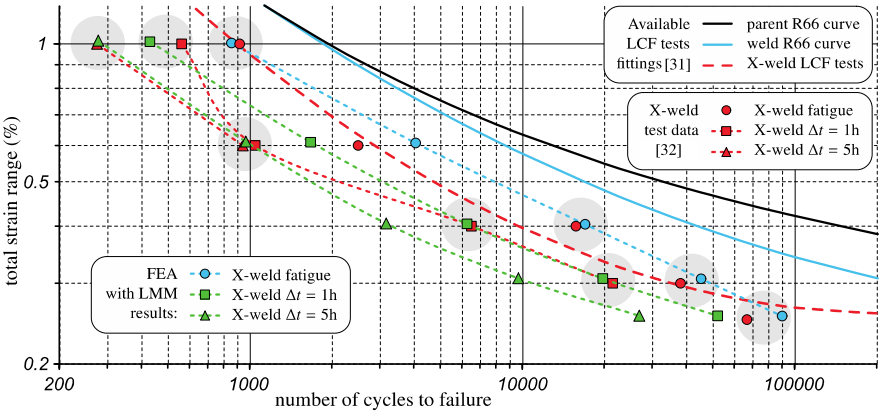

Fig. 10 Results of creep-fatigue assessment in application to cruciform weldment and comparison with experiments [31, 32]

A Ramberg-Osgood formulation was adopted to simulate cyclic stress strain relationship, and a time hardening creep constitutive model was used to characterise creep behaviour. In this creep fatigue damage assessment, the LMM was adopted to evaluate a steady-state cyclic behaviour and to construct a saturated hysteresis loop. Then obtained total strain range during the cycle was used to assess fatigue damage combining R6 fatigue endurance curves [31]. The evaluated creep strain and stress relaxation data were adopted to evaluate creep damage considering time fraction rule and using the experimental creep rupture data. The final lifetime of the cruciform weldment was then obtained based on the calculated fatigue and creep damage under creep-fatigue interaction conditions.

The detailed results of cruciform weldment creep fatigue assessment by the LMM and comparisons with experimental solutions [32] are presented in Fig. 10. Visual comparison of the observed and predicted in Fig. 10 for 3 variants of dwell period Δt shows that 9 of the 11 simulations accurately predict the experimental results. Therefore, it can be used for the formulation of an analytic assessment model suitable for the fast estimation of lifetime for a variety of loading conditions. The low computational effort required by the LMM compared to other computational techniques makes it possible and relatively easy to extrapolate numerical predictions for loading conditions not captured by the available experiments.

A full discussion of the solutions and validations with experimental results are given by Gorash and Chen [33]. This example demonstrates that, for such complex industrial problems, the LMM is capable of providing lifetime related solutions that are much more illuminating than conventional analysis.

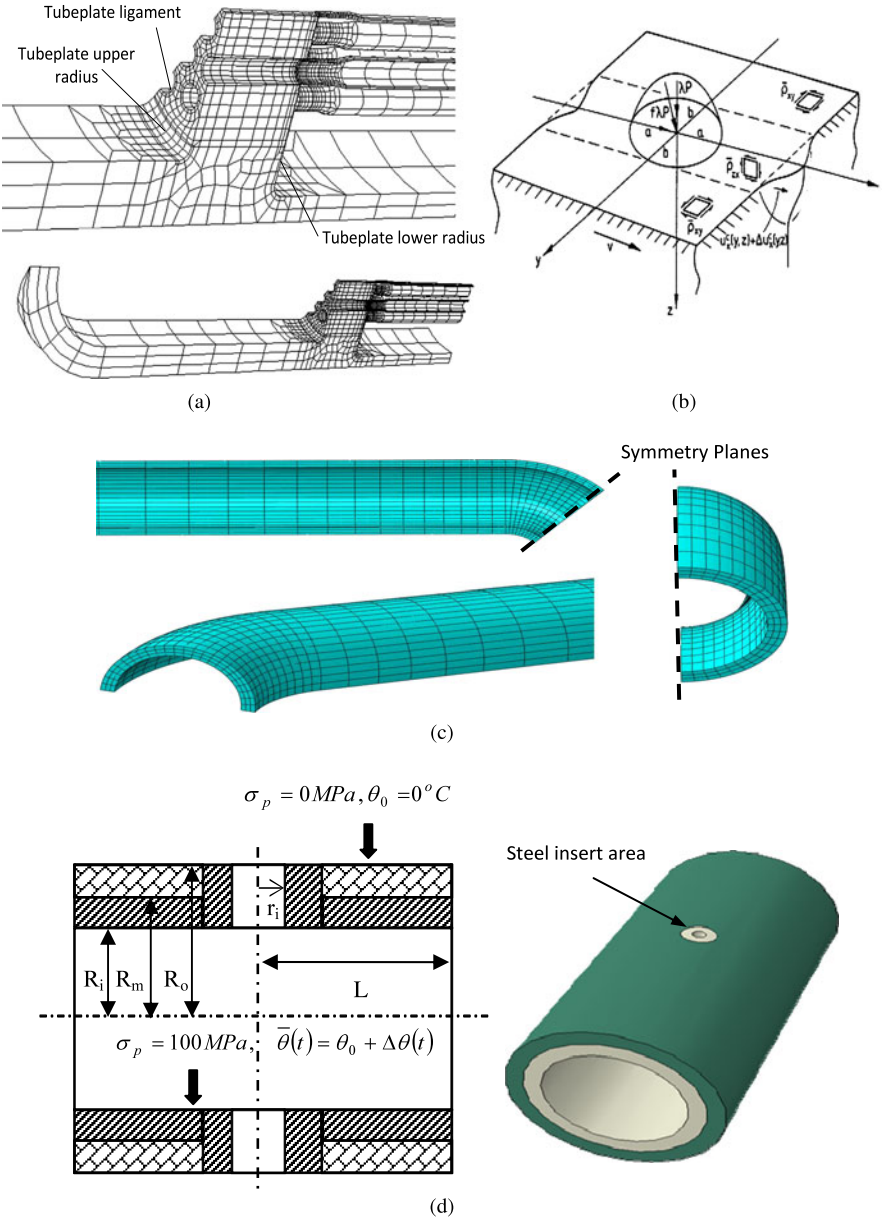

Fig. 11 Other applications (**a**) a heat exchanger tube plane (**b**) rolling contact problem (**c**) 90 pipe bends (**d**) composite cylinder with a crosshole

8 Other Applications

The stable and accurate results of the mentioned LMM on shakedown and ratchet analysis have been confirmed in many industrial applications, including the problem of a heat exchanger tube plate subjected to severe cyclic thermal loading and constant operating pressure (Fig. 11(a)) [8], the application to rolling contact problem (Fig. 11(b)) [34], shakedown and limit analysis of 90 pipe bends under internal pressure, cyclic in-plane bending and cyclic thermal loading (Fig. 11(c)) [35], and the shakedown analysis of a composite cylinder with a cross hole (Fig. 11(d)) [36] and etc.

9 Conclusions

This study focuses on the performance of an elastic plastic body subjected to cyclic loading. The design limits in plasticity and creep including shakedown limit, ratchet limit, cyclic response under creep-fatigue interaction and plastic strain range regarding the fatigue crack initiation have been addressed in this study. The analysis is performed by describing the steady cyclic state employing a general cyclic minimum theorem. In order to estimate the class of kinematically allowable strain rate histories, the Linear Matching Method is used for obtaining the minimum of the functional for these design limits. Three practical examples of the LMM are provided to confirm the efficiency and effectiveness of the method and demonstrate that the LMM may be applied to a much wider range of circumstances than have hitherto been possible.

Acknowledgements The author gratefully acknowledges the support of the Engineering and Physical Sciences Research Council (EP/G038880/1) of the United Kingdom, and the University of Strathclyde during the course of this work. The author would also like to thank Prof Alan Ponter of the Department of Engineering, Leicester University, for his advice and discussion on the theoretical development of the LMM.

References

1. ABAQUS (2007) User's manual. Version 6.7
2. Nguyen-Tajan TMI, Pommier B, Maitournam H, Houari M, Verger L, Du ZZ et al (2003) Determination of the stabilized response of a structure undergoing cyclic thermal–mechanical loads by a direct cyclic method. In: ABAQUS users' conference proceedings
3. Carter P (2005) Analysis of cyclic creep and rupture, part 2: calculation of cyclic reference stresses and ratcheting interaction diagrams. Int J Press Vessels Piping 1(82):27–33
4. Ponter ARS, Carter KF (1997) Limit state solutions, based upon linear elastic solutions with a spatially varying elastic modulus. Comput Methods Appl Mech Eng 140:237–258
5. Ponter ARS, Engelhardt M (2000) Shakedown limits for a general yield condition: Implementation and application for a von-Mises yield condition. Eur J Mech Appl Solids 19:423–445
6. Ponter ARS, Chen HF (2001) A minimum theorem for cyclic load in excess of shakedown, with application to the evaluation of a ratchet limit. Eur J Mech Appl Solids 20:539–553

7. Chen HF, Ponter ARS (2001) A methodfor the evaluation of a ratchet limit and the amplitude ofplastic strain for bodies subjected to cyclic loading. Eur J Mech Appl Solids 20:555–571
8. Chen HF, Ponter ARS (2005) Interity assessment of a 3D tube plate using the linear matching method, creep relaxation and reverse plasticity. J Press Vessel Technol 82:85–104
9. Chen HF, Ponter ARS (2003) Methods for the evaluation of creep relaxation and the amplitude of strains for bodies reverse-plastic strains for bodies reverse-plastic subjected to cyclic loading. In: Pressure vessels and piping, transaction of the ASME, Cleveland, OH, July 2003
10. ANSYS Inc. Southpointe, 275 Technology Drive, Canonsburg, PA 15317. www.ansys.com
11. Hibbit, Karlson and Sorensen Inc (1997) ABAQUSIStandard user's manual, version 6.1, vols 1, 2 & 3. USA
12. ASME (1990) Boiler and pressure vessel code. Code case: nuclear components, case N-47-29, class I components in elevated temperature service. Sect 11, division I
13. AFCEN (1985) Design and construction rules for mechanical components of FBR nuclear islands. RCC-MR, AFCEN, Paris
14. Liu YH, Carvelli V, Maier G (1997) Integrity assessment of defective pressurized pipelines by direct simplified methods. Int J Press Vessels Piping 74:49–57
15. Vu DK, Yan AM, Nguyen DH (2004) A primal–dual algorithm for shakedown analysis of structures. Comput Methods Appl Mech Eng 193:4663–4674
16. Staat M, Heitzer M (2001) LISA a European project for FEM-based limit and shakedown analysis. Nucl Eng Des 206:151–166
17. Seshadri R (2005) Inelastic evaluation of mechanical and structural components using the generalized local stress strain method of analysis. Nucl Eng Des 153:203–287
18. Mackenzie D, Boyle JT, Hamilton R, Shi J (1996) Elastic compensation method in shell-based design by analysis. In: Proceedings of the 1996 ASME pressure vessels and piping conference, vol 338, pp 203–208
19. Chen HF, Ponter ARS, Ainsworth RA (2006) The linear matching method applied to the high temperature life integrity of structures, part 1: assessments involving constant residual stress fields. Int J Press Vessels Piping 83(2):123–135
20. Chen HF, Ponter ARS, Ainsworth RA (2006) The linear matching method applied to the high temperature life integrity of structures, part 2: assessments beyond shakedown involving changing residual stress fields. Int J Press Vessels Piping 83(2):136–147
21. Ainsworth RA (ed) (2003) R5: assessment procedure for the high temperature response of structures. British Energy Generation Ltd, London, p 3
22. Bree J (1967) Elastic-plastic behaviour of thin tubes subjected to internal pressure and intermittent high-heat fluxes with application to fast-nuclear-reactor fuel elements. J Strain Anal 2:226–238
23. Bree J (1989) Plastic deformation of a closed tube due to interaction of pressure stresses and cyclic thermal stresses. Int J Mech Sci 31(11–12):865–892
24. Chen HF, Ponter ARS (2010) A direct method on the evaluation of ratchet limit. J Press Vessel Technol 132:041202
25. Koiter WT (1960) General theorems for elastic plastic soloids. In: Sneddon JN, Hill R (eds) Progress in solid mechanics, vol 1. North Holland, Amsterdam, pp 167–221
26. Melan E (1936) Theorie statisch unbestimmter Systeme aus ideal-plastischem Bastoff. Sitzungsber Akad Wiss Wien, Abtiia 145:195–218
27. Chen HF, Ponter ARS (2006) Linear matching method on the evaluation of plastic and creep behaviours for bodies subjected to cyclic thermal and mechanical loading. Int J Numer Methods Eng 68:13–32
28. Chen H, Chen W (2012) A direct method on the evaluation of cyclic behaviour with creep effect. In: Proceedings of the ASME 2012 pressure vessels & piping division conference, Toronto, ON, Canada, 15–19 July 2012
29. Chen H, Chen W, Li T, Ure J (2011) On ratchet, shakedown and limit analyses of defective pipeline. J Press Vessel Technol
30. Chen H, Chen W, Li T, Ure J (2011) Effect of circular holes on the ratchet limit and crack tip plastic strain range in a centre cracked plate. Int J Fract Mech 78:2310–2324

31. Bate SK, Hayes JP, Hooton DG, Smith NG (2005) Further analyses to validate the R5 volume 2/3 procedure for the assessment of austenitic weldments. Report for British Energy Generation Ltd No SA/EIG/11890/R002, Serco Assurance, Warrington, UK
32. Bretherton I, Knowles G, Hayes JP, Bate SK, Austin CJ (2004) Final report on the fatigue and creep fatigue behaviour of welded cruciform joints. Report for British Energy Generation Ltd No RJCB/RD01186/R01, Serco Assurance, Warrington, UK
33. Gorash Y, Chen HF (2012) Creep fatigue life assessment of cruciform weldments using the linear matching method. Int J Press Vessels Piping 104:1–13
34. Chen H, Ponter ARS (2005) The linear matching method for shakedown and limit analysis applied to rolling and sliding point contact. Road Mater Pavement Des 6:9–30
35. Chen H, Ure J, Li T, Chen W (2011) Shakedown and limit analysis of 90° pipe bends under internal pressure, cyclic in-plane bending and cyclic thermal loading. Int J Press Vessels Piping 88:213–222
36. Chen H, Chen W, Li T, Ure J (2011) Shakedown analysis of composite cylinders with cross hole. J Press Vessel Technol 133:031206